Sheridan College

SOURCE: Sheridan Scholarly Output Undergraduate Research Creative Excellence

Faculty Publications and Scholarship   School of Chemical and Environmental Sciences

4-2010

Numerical Modeling and Experimental Investigation of Gas-Liquid Slug Formation in a Microchannel T-Junction

Rafael M. Santos
University of Toronto, rafael.santos@sheridancollege.ca

Masahiro Kawaji
University of Toronto

Follow this and additional works at: http://source.sheridancollege.ca/fast_chem_publ

Part of the Chemical Engineering Commons

Numerical modeling and experimental investigation of gas-liquid slug formation in a microchannel T-junction

Rafael M. Santos*, Masahiro Kawaji

Department of Chemical Engineering and Applied Chemistry, University of Toronto, 200 College Street,

Toronto, Ontario, M5S 3E5, Canada

Abstract

Gas-liquid two-phase flow in a microfluidic T-junction with nearly square microchannels of 113 μm hydraulic diameter was investigated experimentally and numerically. Air and water superficial velocities were 0.018–0.791 m/s and 0.042–0.757 m/s, respectively. Three-dimensional modeling was performed with computational fluid dynamics (CFD) software FLUENT and the volume-of-fluid (VOF) model. Slug flow (snapping/breaking/jetting) and stratified flow were observed experimentally. Numerically predicted void fraction followed a linear relationship with the homogeneous void fraction, while experimental values depended on the superficial velocity ratio U_G/U_L. Higher experimental velocity slip caused by gas inlet pressure build-up and oscillation caused deviation from numerical predictions. Velocity slip was found to depend on the cross-sectional area coverage of the gas slug, the formation of a liquid film and the presence of liquid at the channel corners. Numerical modeling was found to require improvement to treat the contact

1

angle and contact line slip, and could benefit from the use of a dynamic boundary condition to simulate the compressible gas phase inlet reservoir.

* Corresponding author.

E-mail address: rafael.santos@alumni.utoronto.ca (R.M. Santos).

1. Introduction

Multiphase flow in microchannels has gained much interest in recent years given the numerous emerging applications of microfluidics that promise to provide technological innovations not realizable with conventional channels. Gas-liquid two-phase flows in microchannels often exhibit different flow behaviour than macro-sized conduits, which allows for the precise control of the trajectory of fluidic particles. Significant developments in the area of micro-scale fabrication have allowed researchers to construct increasingly more intricate devices.

Lab-on-a-chip devices have been constructed for use in the biomedical field to perform DNA analysis, enzymatic analysis, proteomics, immunoassaying and point-of-care clinical pathology (Freire and Wheeler, 2006). Microchannels have also been used to study the flow characteristics of microgel capsules and optimize their use for drug delivery in live tissues (Fiddes et al., 2007). Cabral and Hudson (2006) developed a microfluidic multicomponent interfacial tensiometer capable of handling a high-throughput of complex fluids.

The successful design of microfluidic devices relies on the need to fully understand the flow dynamics and physics, obtained mainly by experimental means and in a more limited form from numerical modeling. However, large discrepancies still exist in the published data, largely as a result of difficulty and inconsistencies in experimental setup and measurement. The accuracy and reliability of present correlations and models could be extensively improved if the intricacies of the flow fields were known in more detail, which has recently become possible with the advances in the field of multiphase computational fluid dynamics (CFD).

2

The main objective of the present study is to perform systematic modeling and experimentation of gas-liquid two-phase flow in a microfluidic T-junction channel geometry, and compare their results in order to obtain comprehensive understanding of the flow characteristics at the micro-scale. Moreover, this study also provides the opportunity to put to the test the present state of multiphase CFD modeling and provide insight into its suitability for simulating microfluidic multiphase flow, the accuracy of its predictions, and the limitations that still need to be addressed.

2. Background

The different flow behaviour in microchannels is often attributed to the increased importance and effect of surface tension forces at micro-scales, while gravitational forces become negligible, and inertial, shearing and drag forces have a limited effect (Brauner and Moalem-Maron 1992, Akbar et al. 2003, Garstecki et al. 2006). The wetting properties of the fluids relative to the channel walls, more specifically the contact angle, have also been shown to affect the two-phase flow patterns in microchannels (Rosengarten et al. 2006)

Flow patterns that have been identified in microfluidic gas-liquid two-phase flow include bubbly, slug, ring, churn and annular flow (Kawahara et al. 2002). In some cases a thin film of liquid has been observed between the bubble and the channel wall (Irandoust et al. 1989, Rosengarten et al. 2006, Fukagata et al. 2006, Taha and Cui 2006). Over a specific range of operating conditions and using an appropriate combination of channel geometry and inlet conditions, it is possible to restrict the two-phase flow pattern in microchannels to the regime called Taylor slug flow, where the gas phase takes the form of elongated bubbles of characteristic capsular or bullet shapes, which occupy the entire cross-sectional area of the channel and are separated from each other by liquid plugs.

Compared to single phase laminar flow, Taylor slugs have been shown to increase transverse mass and heat transfer because of recirculation within the liquid plugs and the reduction of axial mixing between liquid plugs (Irandoust et al. 1989). Literature results indicate that the mass transfer, pressure drop and resident time distribution are dependent on the slug length and liquid film thickness; however these two quantities cannot be determined a priori, making the operation of microfluidic devices highly dependent on empirical correlations and modeling results (Qian and Lawal 2006).

Several techniques have been developed to produce gas slugs using different microchannel geometries. Gañán-Calvo and Gordillo (2001), Cubaud and Ho (2004) and Cubaud et al. (2005) described a method using capillary hydrodynamic flow focusing, Yasuno et al. (2004) proposed a microchannel emulsification method, Kawahara et al. (2002), Serizawa et al. (2002) and Xiong and Chung. (2007) used millimeter-sized orifice mixers to produce a pre-mixed two-phase flow that later entered a microchannel capillary, Xu et al. (2006) used a cross-flowing shear-rupturing method, and Xiong et al. (2007) used co-flowing channels. The T-junction gas slug break-up method, whereby channels of equal hydraulic diameter carry the gas and liquid phases that meet in a perpendicular junction, has become widely popular in recent studies (Thorsen et al. 2001, Okushima et al. 2004, Günther et al. 2004, Garstecki et al. 2006, Ide et al. 2007b).

While experimental work on gas-liquid two-phase flow in microchannels is abundant, that is not the case for numerical modeling of the same process. In recent years the first numerical results have been published on slug formation and flow in microfluidic geometries. Some notable studies are those of Tatineni and Zhong (2005), Taha and Cui (2006), Xiong et al. (2007), Qian and Lawal (2006), Fukagata et al. (2007) and Akbar and Ghiaasiaan (2006). The first three performed three-dimensional modeling of slug formation using flow focusing, slug movement within capillaries, and co-flowing channels respectively, while the next two works used a two-dimensional model to simulate the slug formation in a microchannel T-junction.

In the present study Taylor slugs were experimentally produced in a microfluidic chip with a T-junction microchannel geometry. Numerical modeling, using the commercial computational fluid dynamics software FLUENT was performed of the same channel geometry using flow parameters identical to the experimental values. Modeling was entirely done in three-dimensional fashion, in order to fully capture the interfacial tension forces that are dominant in the slug break-up process. Numerical and experimental data were compared to published results in order to gain insight into the slug formation mechanisms and bring consensus into the field.

3. Experimental Setup and Procedure

The microfluidic chip consisted of a main microchannel of overall length of 60 mm and a side stream making up the tee having a length of 30 mm and located at the center of the main channel. The microchannels had rectangular cross-sections, and the respective widths of the inlet, side and outlet channels were: 111, 118 and 108 μm. The depth of each channel was 119 μm. The static contact angle of the microchannel interior was measured using the method described by Hoffman (1975) for a meniscus inside a capillary tube. Ten measurements were made, yielding an average value of 36.4°, with an uncertainty of ±3.8°.

The fluid delivery method of the experimental apparatus consisted of two independent syringe pumps (Cole Palmer; RK-74900-00; specified accuracy ±0.5%) driving the plungers of gas-tight syringes (Hamilton Company; 1, 2.5, 5, 10 ml) containing the chosen immiscible phases: deionised water (the liquid continuous phase, introduced via the main channel inlet) and air (the gas dispersed phase, introduced via the side channel inlet). The syringes were connected to the microchannels by Teflon tubing (Hamilton Company; gauge 13). The two-phase flow formation at the T-junction was imaged via a CCD camera (Pulnix; TM-1040) at 30 fps and 1/16,000 shutter speed with a 5x magnification lens (Mitutoyo; M Plan APO 5) and with background lighting (Schott-Fostec; DCR III Plus). The experimental setup is illustrated in Figure 1.

For each experimental run a consistent start-up procedure was used in order to ensure reliable and accurate data collection and to ensure that only the modified flow variables affected the outcome of each run. The steady slug formation stage of the experimental run typically lasted 5 minutes and sets of 30 images were collected at 20-second intervals.

4. Numerical Methods

FLUENT 6.2 CFD software was used to model slug formation in the microfluidic T-junction. The Volume of Fluid (VOF) model in three-dimensional form was used, which enables capturing and tracking the precise location of the interface between the fluids. The VOF method operates under the principle that the two or more fluids are not interpenetrating. For each qth fluid phase in the system a new variable is introduced called the volume fraction (Ω_q). For each computational control volume the sum of all volume fractions must equal to unity. All variables and properties (such as density ρ, and dynamic viscosity μ) in any computational

cell are volume-averaged values, such that they are either representative of a single pure phase (when $\Omega_q = 0$ or $\Omega_q = 1$), or are representative of a mixture of the phases (at phase interfaces when $0 > \Omega_q > 1$).

A single continuity equation (1) and the momentum equation (2) are solved continuously across the computational domain. The VOF method accomplishes interface tracking by solving an additional continuity-like equation (3) for the volume fraction of the primary phase (gas), which yields the value of Ω_G. Ω_L is computed as $1 - \Omega_G$. The body force term (F) in Equation (2) is responsible for taking into account the surface tension (σ) and contact angle (θ) effects, and it is computed in FLUENT by use of the Continuum Surface Force (CSF) model (Brackbill et al. 1992). This model, rather than imposing the contact angle effect as a boundary condition at the wall, uses the contact angle value to adjust the interface normal in cells near the wall.

$$\frac{\partial \rho}{\partial t} + \nabla \cdot \left(\rho \vec{v} \right) = 0 \tag{1}$$

$$\frac{\partial \left(\rho \vec{v} \right)}{\partial t} + \nabla \cdot \left(\rho \vec{v} \vec{v} \right) = -\nabla \rho + \nabla \cdot \left[\mu \left(\nabla \vec{v} + \nabla \vec{v}^T \right) \right] + \vec{F} \tag{2}$$

$$\frac{\partial \Omega_G}{\partial t} + \vec{v} \cdot \nabla \Omega_G = 0 \tag{3}$$

A segregated axisymmetric time-dependent unsteady solver was used along with the implicit body force formulation. For discretization the PRESTO! (Pressure staggering options) scheme was used for pressure interpolation, the PISO (Pressure-implicit with splitting of operators) scheme was used for pressure-velocity coupling, and the second-order up-wind differencing scheme was used for the momentum equation. Air was designated as the primary phase and water as the secondary phase. Wall adhesion was turned on so that the contact angle ($\theta = 36°$) could be prescribed and a constant surface tension value ($\sigma = 73.5$ dyn/cm) was inputted. For the inlets, the velocity inlet boundary condition was used, while pressure outlet boundary condition was used for the outlet. Numerical runs were performed remotely in batch mode at the HPCVL (High Performance Computing Virtual Laboratory) facility located at Queen's University.

The computational mesh was prepared using the Gambit 2.3 software (Fluent Inc.). Quadrilateral elements were used with the paved meshing scheme and a mesh spacing of 5.67 µm. Preliminary numerical

runs were performed to ensure the flow dynamics were independent of mesh resolution. The full computational mesh for the microfluidic T-junction is shown in Figure 2 along with the dimensions of the channels. The lengths of the inlet channels were chosen according to the necessary lengths required for full laminar flow to develop prior to the T-junction. The outlet channel was made long enough so that in most numerical runs more than one gas slug would form in the field of view.

5. Effect of Computational Dimensions

A large portion of computational fluid dynamics (CFD) modeling in the literature has been performed with two-dimensional models, leaving only a fraction of problems being solved with full three-dimensionality. The principal reason for this is that three-dimensional models increase the computational costs dramatically, resulting in the need for larger computer memories and in longer computational times. However, for multiphase flow problems, the third dimension in many cases cannot be disregarded. This is especially true when interface tracking is to be accomplished.

In the case of formation of gas slugs in a microfluidic T-junction, gas slugs break off due to the narrowing of the fluid region connecting the gas slug to gas inlet region. In the break-up of a two-dimensional system, such as a liquid sheet, the dominant factors contributing to the narrowing process are the growth of instabilities, viscous and kinetic effects. In three-dimensional systems, such as liquid jets, the surface tension becomes a much more important factor. As necking of the jet occurs, surface tension forces exist in all radial directions pointing inward, thus leading to the growth of the oscillation amplitude and the eventual pinching of the jet and formation of a drop or bubble. In comparison, for a 2D case, the surface curvature only exists in one dimension, and the surface tension components on either side of the fluid point in the opposite direction, stabilizing the oscillation effect (Ashgriz, 2006). As a result it becomes intuitive that for the study of slug formation in a microchannel a fully three-dimensional model may capture the slug formation physics more accurately.

To test the effect of the third dimension, numerical runs were performed using the same flow, mesh and solver parameters for both a 2D and 3D model. It was found that at higher shearing rates, the model predictions differ substantially, as shown in the resulting phase contour plots in Figure 3. In particular, while

in the 3D case several slugs were formed for flow condition of 0.5 m/s gas inlet velocity, in the 2D case the gas slug is still stretched and has not pinched off. Also, it can be noted that in the case of gas velocity of 0.2 m/s, the gas slug in the 2D case does not acquire a spherical shape due to the lack of Laplace pressure, which would cause the interface to become more rigid and spherical. Due to these differences, the modeling in this work as performed solely in 3D.

6. Flow Conditions

A total of 30 experimental and numerical runs were performed using the same flow conditions for direct comparison of results. Gas superficial velocities (U_G) ranged from 0.018 m/s to 0.791 m/s, and liquid superficial velocities (U_L) ranged from 0.042 m/s to 0.757 m/s.

Table 1 presents ranges of values for commonly reported non-dimensional parameters for gas and liquid flow in microfluidic channels. These include the Bond number (Bo; ratio of gravitational force to surface tension force), the Capillary number (Ca; ratio of viscous force to surface tension force), the Reynolds number (Re; ratio of inertia force to viscous force) and the Weber number (We; ratio of inertia force to surface tension force). U_{tot} is the total outlet superficial velocity, equal to the sum of gas and liquid superficial velocities, D_h is the hydraulic channel diameter, and g is the gravitational acceleration.

Upon inspection of the non-dimensional parameters it becomes clear that surface tension forces are dominant at the present microfluidic dimensions. A criterion proposed by Brauner and Moalem-Maron (1992) is that when Bo $<< (2\pi)^2 \approx 39.5$ surface forces become dominant over gravity, and gravitational forces can be neglected. This is the case with the present flow rates, hence gravitational forces were neglected in the numerical code. Furthermore, Tice et al. (2003) indicated that droplets with diameters smaller than the channel dimensions form when Ca > 1. In the present case, where Ca < 0.02, it is thus expected that no droplets smaller than the channel cross-section form. One more relation to the Capillary number is discussed by Garstecki et al. (2006), who postulated that a critical Capillary number exists above which shear stresses begin to play an important role in the process of droplet break-up, as opposed to necking by pressure squeezing. The proposed critical value of Ca $\sim 10^{-2}$ is not exceeded in most of the present runs. The values of the Weber number can be compared with a correlation fitted by Akbar et al. (2003) that specifies the surface

tension dominated region, as indicated by a slug flow pattern in mini- and micro-channels when $We_G \leq$ $0.11We_L^{0.315}$. All runs in the present work have Weber numbers that obey this limit. Lastly, Reynolds numbers are well into the laminar flow region, as is the case with most flows at the microfluidic scale given the small channel dimensions used.

7. Results and Discussion

7.1 Experimental Results

7.1.1 Analytical Modeling of Start-up Stage

During start-up, the gas within the syringe and tubing was compressed and became pressurized. This inlet gas pressure build-up affects the flow pattern and dynamics in the microchannel and creates challenges for producing accurate modeling results. To gain insight into this process, the pressure of each stream during start-up was analytically modeled using the Darcy-Weisbach equation for laminar flow. The pressure loss of the outlet stream was equalized with the sum of the pressure loss and gas static pressure on the side stream, allowing for the determination of the inlet gas static pressure (P_G) and gas density (ρ_G) for each experimental run at the moment the first gas slug formed at the T-junction. This model was verified by comparing the calculated duration of the start-up stage with experimentally measured values. The maximum inlet gas gauge pressure obtained was 117.6 kPa ($\rho_G = 2.60$ kg/m^3), and the minimum value was 5.3 kPa ($\rho_G = 1.27$ kg/m^3).

The calculated initial inlet gas gauge pressure divided by the inlet gas superficial velocity (U_G) correlates well with the gas-to-liquid ratio of inlet superficial velocities (U_G/U_L), as shown in Figure 4. For U_G much larger than U_L, the gas pressure increases only slightly over atmospheric, as result of a brief start-up period (gas flow quickly pushed the liquid back into the microchannel, and slug formation commenced promptly). On the other hand, when the gas flow rate was smaller than the liquid flow rate, liquid initially entered the gas inlet line and it took a significantly larger period of time for slug formation to begin, resulting in considerable gas pressurization.

7.1.2 Experimental Flow Patterns

In the present study, two types of flow patterns were observed: slug flow and stratified flow. Furthermore, during slug flow, it was observed that the slugs are produced in three different manners at the T-junction, and the patterns are referred to as: breaking slug formation, snapping slug formation and jetting slug formation. Typical images of each flow pattern are shown in Figure 5.

In the case of breaking slug flow the gas slug exits the gas inlet channel and flows close to the top channel wall, forming a single contact point, while the liquid stream pushes the slug forward and passes underneath it. The slug breaks off once the surface tension force can no longer hold the slug connected to the inlet stream, resulting in necking and break off. The liquid flow may at the same time push the interface towards the top wall, which touches the corner of the T-junction and clips off prematurely.

During snapping slug formation, the slug touches both the top and bottom channel walls while it is still growing, blocking the entire channel cross-section (except perhaps for the channel corners, which cannot be assessed by these images). As a consequence three interface contact points with the wall form: two at the front nose and one at the bottom rear. The slug continues to grow and move downstream, stretching the tail that is still connected to the gas inlet stream. Once the tail thins it snaps, creating a fourth contact point of the slug interface with the wall; at the same time, the gas tail retracts to the T-junction.

The gas slug formation referred to here as the jetting slug formation is unique in that the gas stream protrudes into the main channel as a finger-like fluid structure oriented towards the channel outlet. From its end, gas slugs pinch off in a manner similar to instability propagation typically found in formation of bubbles or drops from jets.

Finally, a stratified flow pattern was also observed in some experimental runs in conjunction with the slug flow pattern, alternating with time. This flow pattern is characterized by the gas flowing in parallel with the liquid phase. The width of the gas stream varied, in some cases reaching approximately half the channel width, and the interface remained nearly straight or oscillated in a wave-like pattern. This flow pattern appeared to be related to the pressure build-up in the gas inlet line. In certain conditions the stratified flow stretched the entire length of the microchannel, connecting the open atmosphere to the gas reservoir and leading to its depressurization, after which the flow pattern returned to slug flow.

The flow patterns were correlated with the inlet superficial velocities to produce a flow pattern map, shown in Figure 6. The snapping regime predominates at low liquid superficial velocities. At higher liquid velocities the flow transitions to the breaking regime, which alternates with stratified flow at intermediate to high gas velocities. The jetting regime appears for the combination of high liquid and gas velocities.

7.2 Comparison of Experimental and Numerical Results

7.2.1 Void Fraction

The void fraction (ε) is essentially a measure of the fraction of channel volume occupied by the gas phase, and is a useful measure of assessing the behavior of slug flow in a microfluidic channel. Work has been done by a number of researchers on the acquisition of void fraction correlations from experiments. Armand (1946) proposed a relationship for conventional tubes in the form of Equation (4), where β is the homogeneous void fraction (5).

$$\varepsilon = 0.833\beta \qquad (4)$$

$$\beta = \frac{U_G}{U_G + U_L} \qquad (5)$$

Kawahara et at. (2002) measured void fraction in a circular microchannel of 100 μm diameter. Air and water were pre-mixed in a mixer of 0.5 mm channel diameter before entering the microchannel. The flow conditions produced a rapidly variable array of flow patterns other than pure slug flow, including primarily gas-core flow with a smooth or wavy liquid film flowing along the channel wall. Their void fraction data deviated significantly from Armand's correlation, yielding a correlation that predicted much lower ε values up to high values of β (6). This deviation was likely caused by the introduction of gas and liquid in a pre-mixer substantially larger than the microchannel. This caused the formation of an alternating gas-liquid flow regime in the microchannel rather than Taylor slug flow. As a result of lower pressure drop during predominantly gas-core flow, the gas passed the microchannel much faster than the liquid phase (high velocity slip) and the observed void fraction decreased considerably.

$$\varepsilon = \frac{0.03\beta^{0.5}}{1 - 0.97\beta^{0.5}} \qquad (6)$$

The experimental void fraction in the present study was determined by analyzing images of the flow, such as to obtain time-averaged void fraction data. The rightmost edge of the channel flow was chosen to be a reference location. The number of images that contained a gas slug crossing the reference location was tallied, and the void fraction resulted in this sum being divided by the total number of images.

Values of void fraction where obtained from numerical results by dividing the volume of a single gas slug (V_S) by the volume occupied by a slug unit (consecutive gas and liquid slugs), according to Equation (7), where L_S is the length of the gas slug, L_C is the length of the liquid slug and A_{ch} is the channel cross-sectional area. Contour plots of the numerical results with the highest and lowest values of ε are displayed in Figure 7.

$$\varepsilon_{num} = \frac{V_S}{\left(L_S + L_C\right) \times A_{ch}} \tag{7}$$

Data from the present study is plotted in Figure 8 alongside curves representing Equations (4) and (6) as a function of the homogeneous void fraction. The numerical simulations predicted a linear relationship with a slope value of 0.95, slightly higher than Armand's correlation. The experimental data was split into two groups. For runs performed where the liquid superficial velocity exceeded the gas superficial velocity ($U_G/U_L < 1$) the data was distributed close to the numerical results. However for runs performed where the gas superficial velocity was greater or equal to the liquid superficial velocity ($U_G/U_L \geq 1$) the data followed a pattern similar to the correlation of Kawahara et al. (2002).

In general, it appears the deviation of microfluidic experimental results from the linear relationship predicted numerically and from conventional channel work is related to the extent of velocity slip (ζ), defined by Equation (8), where v_S is the gas slug velocity, v_C is the liquid slug velocity, and Q_G and Q_L are respectively the gas and liquid volumetric flow rates. On Figure 9 the velocity slip is presented as a function of the superficial velocity ratio U_G/U_L. Less data points are available from numerical simulation given in some numerical runs no more than one gas slug was formed in the channel length modeled, which made it not possible to obtain accurate velocity slip values due to the lack of a complete liquid slug needed to obtain L_C. It is found that the experimental slip is significantly higher when $U_G/U_L \geq 1$, which corresponds to the low void

fraction data that matches results from Kawahara et al. (2002). The numerically predicted slip is significantly less than experimental values when $U_G/U_L \geq 1$, though it also increases as a function of the flow rate ratio.

$$\zeta = \frac{v_S}{v_C} = \frac{Q_G \times (1 - \varepsilon)}{Q_L \times \varepsilon} \tag{8}$$

The discrepancy in velocity slip and void fraction between numerical and experimental data may be a result of two factors. First, the low numerical velocity slip may be caused by the use of a constant contact angle value, which hinders the formation of a complete liquid film around the gas slug. Such film would provide lubrication of the channel wall and enhance velocity slip. Second, and perhaps more important, is the effect of the flow inlet conditions. As mentioned earlier, experimentally the gas inlet initially became pressurized, an effect that was not captured by the incompressible numerical simulation.

Kawahara et al. (2006) have examined the effect of inlet and mixing geometries on the flow behavior in microchannels and have observed that both quasi-separated flow (6) and quasi-homogeneous flow ($\varepsilon \approx \beta$) appear depending on the inlet conditions. Ide et al. (2007) performed experiments in a 100 μm diameter T-junction for two cases of inlet conditions: one where a long compressible air volume existed upstream of the T-junction (case 1), and another where the compressible volume was much smaller (case 2). They found that void fraction data from case 1 correlated well with Equation (6), while case 2 behaved differently, correlating better with the correlation of Armand (1946). They suggested that the void fraction is significantly lowered in case 1 because the flow of gas into the liquid stream at the T-junction is likely intermittent rather than steady, causing long liquid slugs to form. These long liquid slugs would move more slowly than shorter liquid plugs due to increased friction and pressure losses, and as a result the time-averaged void fraction would be reduced.

On Figure 10 it is observed that the experimental velocity slip was greater for flow conditions where the gas stream was least pressurized (that is, lower initial gas density). It may be that at a lower inlet pressure the gas has greater difficulty in accelerating the liquid up to the total superficial outlet velocity (U_L+U_G), which would be required for the slip to be zero. Instead, the gas stream may preferentially penetrate the liquid stream, resulting in gas slugs that travel considerably faster than the continuous phase. As a result the void fraction is lowered and the slip is amplified. Also from Figure 10 it is seen that this low pressure situation

13

coincides with flow conditions where $U_G/U_L \geq 1$, which is the set of data that correlates with the void fraction correlation from Kawahara et al. (2002).

7.2.2 Gas Slug Length

The experimental gas slug lengths (L_S) were measured from several experimental images for each run using image analysis software. Numerical gas slug lengths were computed using a user-defined function in FLUENT. In either case, the gas slug length is taken as the distance between the extremities of a single gas slug. Experimental average gas slug lengths, including error bars, are compared against numerical values on Figure 11. Experimental gas slug lengths ranged from 221 μm to 819 μm, while numerical values ranged from 185 μm to 1912 μm.

It was found that, similarly as in the case of void fraction, for runs where the superficial velocity ratio was $U_G/U_L < 1$ the experimental values were in closer agreement with numerical predictions. When $U_G/U_L \geq 1$, the gas slug lengths increased and the scatter in the data became larger. It is especially evident that when the numerical simulation predicted the longest gas slugs, the experimental equivalents were significantly shorter. This may be caused by increased pressure and flow oscillations resulting from the velocity slip effect discussed earlier related to cases where $U_G/U_L \geq 1$. The increase in error bars lengths can also be attributed to such oscillations. These dynamic effects may lead to premature break-up of the gas slugs, and are not captured in the idealized numerical model. Representative images of experimental and numerical gas slugs are displayed on Figure 12.

The effect of gas and liquid superficial velocities on the gas slug length is presented in Figure 13. In general, larger liquid superficial velocities produced shorter gas slugs, both in experimental and numerical runs. An increase in the gas superficial velocity resulted in longer numerically predicted gas slugs; such effect, however, was not particularly evident in experimental data. The liquid flow may produce pressure and flow disturbances that dominate the slug break-up mechanism, which are not captured numerically due to the use of the incompressible model and fixed velocity boundary conditions.

The actual gas velocity in the inlet channel can differ substantially from the superficial gas velocity thought to be delivered from the syringe pump as a result of the flow disturbances. As such, the gas slug

length produced, which is a direct function of the flow condition at the T-junction, is different from the predicted values based solely on the syringe pump flow rates. Still, it can be said that the numerical model is accurate in capturing two-phase flow physics at the microfluidic scale related solely to flow velocities and surface tension effects, given there are similar trends and response to flow parameters between the numerical predictions and experimental data.

7.3 Cross-sectional Area of Gas Slug

In Taylor slug flow, a gas slug flowing in a microchannel is surrounded by the continuous liquid phase. In a circular microchannel, a lubricating liquid film may coat the channel wall around the gas slug or, depending on the gas slug velocity, Cubaud et al. (2006) have noted that the wall can be dewetted, and a dry gas slug can travel along the channel. In non-circular microchannels (such as square, rectangular and triangular) liquid can also flow along the channel corners, which are more difficult to drain out. As a result a partially lubricated gas slug can also form. The existence of a liquid film between the gas slug and the channel wall affects the occurrence of velocity slip. In the dewetted slug situation, the gas slug must travel at the same velocity as the liquid phase, and hence no velocity slip takes place. In the lubricated slug case (completely or partially), the gas slug can speed up and flow faster than the liquid phase.

In order to investigate how the gas and liquid phases occupy the microchannel it is desirable to observe the area of a plane perpendicular to the fluid flow and measure the cross-sectional gas slug area (A_S). Numerical methods allow for this parameter to be easily be deduced. Data for the present work was obtained using FLUENT by tallying the gas volume fraction (Ω) of 380 node-facets of the plane located at the center of gravity of a gas slug, according to Equation (9).

$$A_S = \frac{\sum_{i=1}^{380} \Omega_{G,i}}{380} \tag{9}$$

From the 30 numerical simulations performed values of A_S ranged from 86% to 100%. Displayed in Figure 14 are two representative contour plots, which show the value of volume fraction of gas at each node-facet of the channel cross-section (these are cell-centered values and node interpolation is turned off to

produce the images). For values below 100% coverage, the gas slug acquires an octagonal shape, with liquid flowing along the channel corners.

The cross-sectional areas occupied by gas slugs can be related to the magnitude of deviation of the gas slug velocity (v_S) from the total outlet superficial velocity (U_{tot}). For the gas slug to flow faster than the liquid phase, liquid must recirculate from the front of the gas slug to its rear, and this is possible due to the existence of liquid flow along the channel corners. The ratio v_S/U_{tot} is plotted as a function of A_S in Figure 15. It is observed that as the gas slug cross-sectional area decreases, the velocity slip increases.

Given experimental results appear to indicate a dominant presence of velocity slip, which was not replicated numerically, it may be reasonable to assume that the flow regime lies in the lubricated slug regime and a liquid film remains on the channel wall. The numerical model predicts a different behavior due to one of more of several factors: (i) inaccurate contact angle value input, (ii) inaccurate surface tension value input, (iii) insufficient grid resolution near the channel wall, (iv) use of incompressible model, (v) lack of dynamic contact angle calculation, or (vi) inadequate modeling of contact line slip. Points i through iv can be verified by further modeling studies, which are ongoing and to be published at a later time.

The latter two points are possible shortcomings of the present version of FLUENT CFD software. Regarding point vi, Rosengarten et al. (2006) have observed that because the contact line must move along the wall, which uses a no-slip boundary condition for fluid flow, the VOF code cannot be truly grid independent. The FLUENT code, which uses the model of Brackbill et al. (1992), allows for the movement of the contact line by computing the mass fluxes from integration over the whole cell adjacent to the wall. A more recent development made by Renardy et al. (2001) could provide a more accurate means of inducing numerical slip.

8. Concluding Remarks

I. Two flow patterns were observed experimentally: slug flow and stratified flow. The slug flow category is further divided into three types of patterns: snapping slug flow, breaking slug flow and jetting slug flow. A flow pattern map was produced showing that each flow pattern occurs for a particular combination of inlet gas and liquid superficial velocities.

16

II. Analyses of non-dimensional parameters according to correlations proposed in the literature were found to be useful for predicting the occurrence and predominance of Taylor slug flow at the flow conditions used in the present study. The prediction of slug flow pattern by numerical simulation also supports the assertion that the CFD code is satisfactorily accurate in predicting microfluidic slug formation.

III. By directly comparing numerical and experimental gas slug lengths, it was observed that gas slugs shorter than 400 μm had similar sizes between the two results, while the longer length results did not match precisely. This discrepancy is likely due to flow disturbances caused at the gas inlet, such as fluid oscillation resulting from pressure changes, which are not captured in the numerical model.

IV. The void fraction was computed numerically and correlated with the homogeneous void fraction in a linear fashion. This result is similar to that predicted by Armand (1946), and is unlike the results of Kawahara et al. (2002) and Xiong and Chung (2007) who obtained much lower void fraction values. The present results confirm observations made by Ide et al. (2007) that the inlet gas condition is critical to determining the extent of velocity slip. In order to accurately model experimental results it may be necessary to introduce a compressible gas volume in the computational geometry, or use a dynamic boundary condition that simulates the gas reservoir effect. Taking into account the idealistic and simplistic nature of the numerical geometry, it appears numerical results calculated by the FLUENT CFD software accurately capture the break-up physics at the microfluidic scale, however improvements could be made to the treatment of contact angle effects and contact line slip.

V. Three-dimensional modeling correctly captured surface tension effects, which are crucial to accurately predicting the formation of two-phase slug flow in a microfluidic T-junction. At higher shearing rates, numerical runs that only utilized two-dimensional models produced slugs of significantly different size, formation frequency and with unusual shapes. Further work is advised to better characterize the differences in the predictions depending on the computational dimensions used.

Acknowledgements

References

Akbar, M.K., and Ghiaasiaan, S.M., 2006. "Simulation of Taylor Flow in Capillaries Based on the Volume-of-Fluid Technique," Industrial & Engineering Chemistry Research 45, 5396-5403.

Akbar, M.K., Plummer, D.A., and Ghiaasiaan, S.M., 2003. On gas-liquid two-phase flow regimes in microchannels. International Journal of Multiphase Flow 29, 855-865.

Ali, M.I., Sadatomi, M., Kawaji, M., 1993. Two-phase flow in narrow channels between two flat plates". Canadian Journal of Chemical Engineering 71, 657-666.

Armand, A.A., and Treschev, G.G., 1946. "The resistance during the movement of a two-phase system in horizontal pipes". Izv. Vse. Tepl. Inst. 1, 16-23.

Ashgriz, N., 2006. Lecture notes, MIE1222 Multiphase Flows, Department of Mechanical and Industrial Engineering, University of Toronto, Toronto, Canada.

Brackbill, J.U., Kothe, D.B., and Zemach, C., 1992. "A Continuum Method for Modeling Surface Tension". Journal of Computational Physics 100, 335-354.

Brauner, N., and Moalem-Maron, D., 1992. "Identification of the range of small diameter conduits, regarding two-phase flow pattern transition". International Communications in Heat and Mass Transfer 19, 29-39.

Cabral, J.T., Hudson, S.D., 2006. "Microfluidic approach for rapid multicomponent interfacial tensiometry". Lab on a Chip 6, 427-436.

Cubaud, T., and Ho, C.-M., 2004. "Transport of bubbles in square microchannels". Physics of Fluids 16, 4575-4585.

Cubaud, T., Tatineni, M., Zhong, X., and Ho, C.-M., 2005. "Bubble dispenser in microfluidic devices". Physical Review E 72, 037302.

Cubaud, T., Ulmanella, U., and Ho, C.-M., 2006. "Two-phase flow in microchannels with surface modifications". Fluid Dynamics Research 38, 772-786.

Fiddes, L., Young, E.W.K., Kumacheva, E., and Wheeler, A.R., 2007. "Flow of Microgel Capsules through Topographically Patterned Microchannels". Lab on a Chip 7, 863-867.

Freire, S., and Wheeler, A.R., 2006. "Proteome-on-a-Chip: Mirage, or on the Horizon?". Lab on a Chip 6, 1415-1423.

Fukagata, K., Kasagi, N., Ua-arayaporn, P., and Himeno, T., 2007. "Numerical simulation of gas-liquid two-phase flow and convective heat transfer in a micro tube". International Journal of Heat and Fluid Flow 28, 72-82.

Gañán-Calvo, A.M., and Gordillo, J.M., 2001. "Perfectly Monodisperse Microbubbling by Capillary Flow Focusing". Physical Review Letters 87, 274501.

Garstecki, P., Fuerstman, M.J., Stone, H.A., and Whitesides, G.M., 2006. "Formation of droplets and bubbles in a microfluidic T-junction – scaling and mechanism of break-up". Lab on a Chip 6, 437-446.

Günther, A., Khan, S.A., Thalmann, M., Trachsel, F., and Jensen, K.F., 2004. "Transport and reaction in microscale segmented gas–liquid flow". Lab on a Chip 4, 278-286.

Hoffman, R.L., 1975. "A study of the advancing interface, Part I: interface shape in liquid–gas systems". Journal of Colloid and Interface Science 50, 228-241.

Ide, H., Kariyasaki, A., and Fukano, T., 2007. "Fundamental data on the gas–liquid two-phase flow in minichannels". International Journal of Thermal Sciences 46, 519–530.

Ide, H., Kimura, R., and Kawaji, M., 2007b. "Effect of inlet geometry on adiabatic gas-liquid two-phase flow in a microchannel". Proceedings of 5th ASME ICNMM.

Irandoust, S., and Andersson, B., 1989. "Liquid film in Taylor flow through a capillary". Industrial and Engineering Chemistry Research 28, 1684–1688.

Kawahara, A., Chung, P.M.-Y., and Kawaji, M., 2002. "Investigation of two-phase flow pattern, void fraction and pressure drop in a microchannel". International Journal of Multiphase Flow 28, 1411-1435.

Kawahara, A., Sadatomi, M., and Kumagae, K., 2006. "Effect of gas-liquid inlet/mixing conditions on two-phase flow in microchannels". Progr. Multiphase Flow Res. I, 197-204.

Okushima, S., Nisisako, T., Torii, T., and Higuchi, T., 2004. "Controlled Production of Monodisperse Double Emulsions by Two-Step Droplet Breakup in Microfluidic Devices". Langmuir 20, 9905-9908.

Qian, D., and Lawal, A., 2006. "Numerical study on gas and liquid slugs for Taylor flow in a T-junction microchannel". Chemical Engineering Science 61, 7609-7625.

Renardy, M., Renardy, Y., and Li, J., 2001. "Numerical Simulation of Moving Contact Line Problems Using a Volume-of-Fluid Method". Journal of Computational Physics 171, 243-263.

Rosengarten, G., Harvie, D.J.E., and Cooper-White, J., 2006. "Contact angle effects on microdroplet deformation using CFD". Applied Mathematical Modelling 30, 1033-1042.

Serizawa, A., Feng, Z., and Kawara, Z., 2002. "Two-phase flow in microchannels". Experimental Thermal and Fluid Science 26, 703-714.

Taha, T., and Cui, Z.F., 2006. "CFD modelling of slug flow inside square capillaries". Chemical Engineering Science 61, 665-675.

Tatineni, M., and Zhong, X., 2005. "Numerical Simulations of Two-Phase Flow in Micro Gas-Liquid Mixing Sections". 43rd AIAA Aerospace Sciences Meeting and Exhibit, 1392.

Thorsen, T., Roberts, R.W., Arnold, F.H., and Quake, S.R., 2001. "Dynamic Pattern Formation in a Vesicle-Generating Microfluidic Device". Physical Review Letters 86, 4163-4166.

Tice, J.D., Song, H., Lyon, A.D., and Ismagilov, R.F., 2003. "Formation of Droplets and Mixing in Multiphase Microfluidics at Low Values of the Reynolds and the Capillary Numbers". Langmuir 19, 9127-9133.

Xiong, R., Bai, M., and Chung, J.N., 2007. "Formation of bubbles in a simple co-flowing micro-channel". Journal of Micromechanics and Microengineering 17, 1002-1011.

Xiong, R., and Chung, J.N., 2007. "An experimental study of the size effect on adiabatic gas-liquid two-phase flow patterns and void fraction in microchannels". Physics of Fluids 19, 033301.

Xu, J.H., Li, S.W., Wang, Y.J., and Luo, G.S., 2006. "Controllable gas-liquid phase flow patterns and monodispersive microbubbles in a microfluidic T-junction device". Applied Physics Letters 88, 133506.

Yasuno, M., Sugiura, S., Iwamoto, S., and Nakajima, M., 2004. "Monodispersed Microbubble Formation Using Microchannel Technique". AIChE Journal 50, 3227-3233.
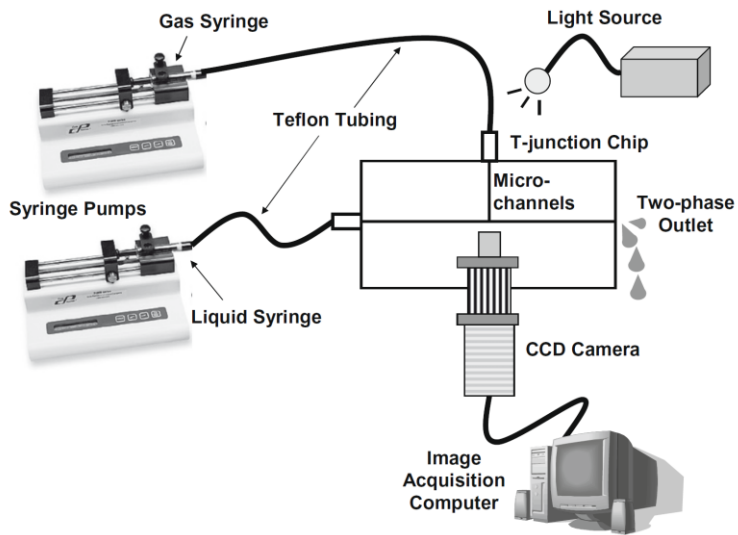
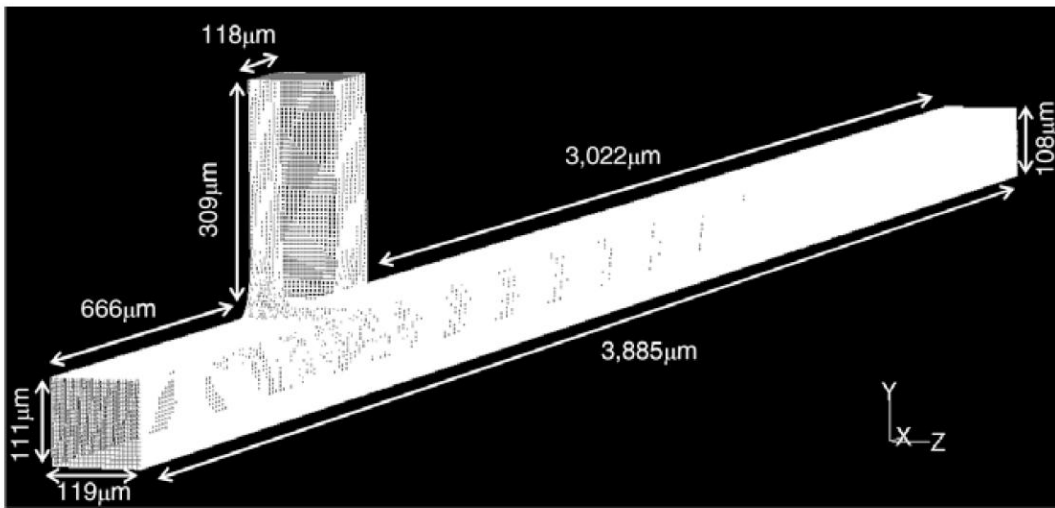Figure 1: Experimental setup

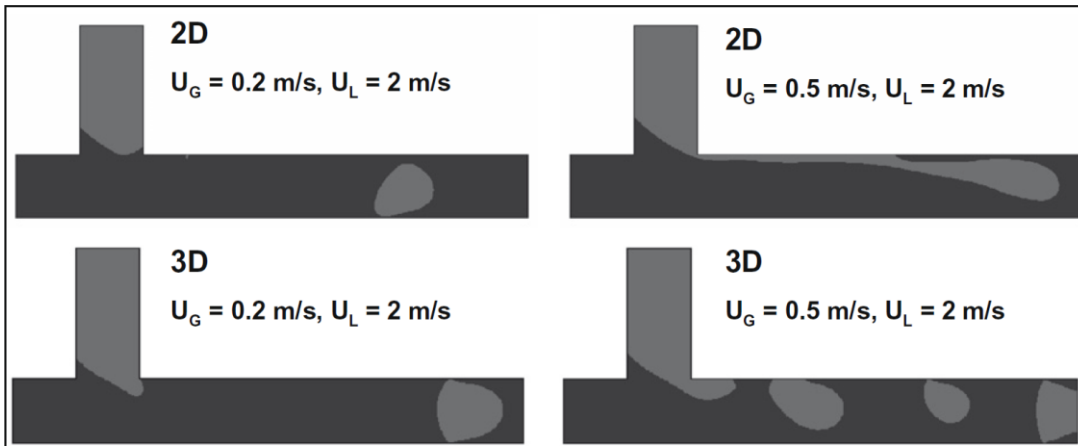Figure 2: Computational T-junction mesh volume

Figure 3: Effect of third dimension on numerical simulation of slug formation
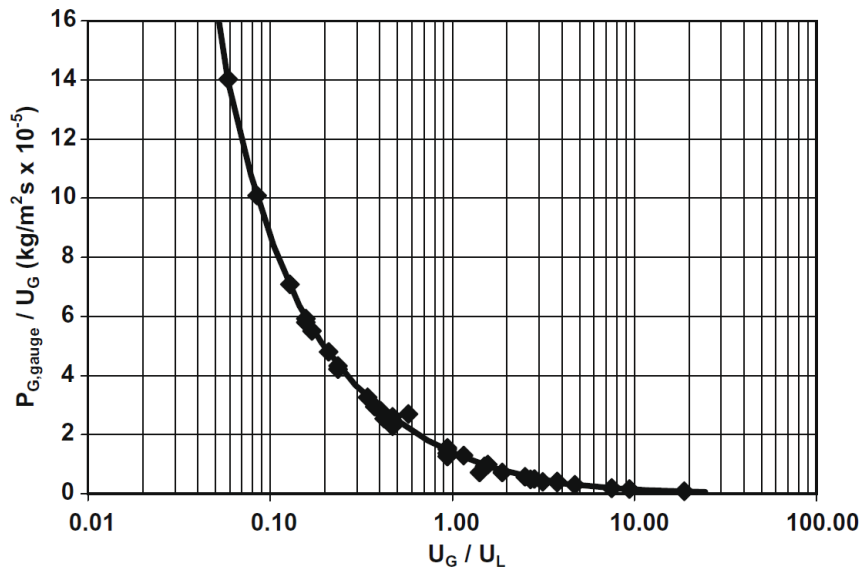

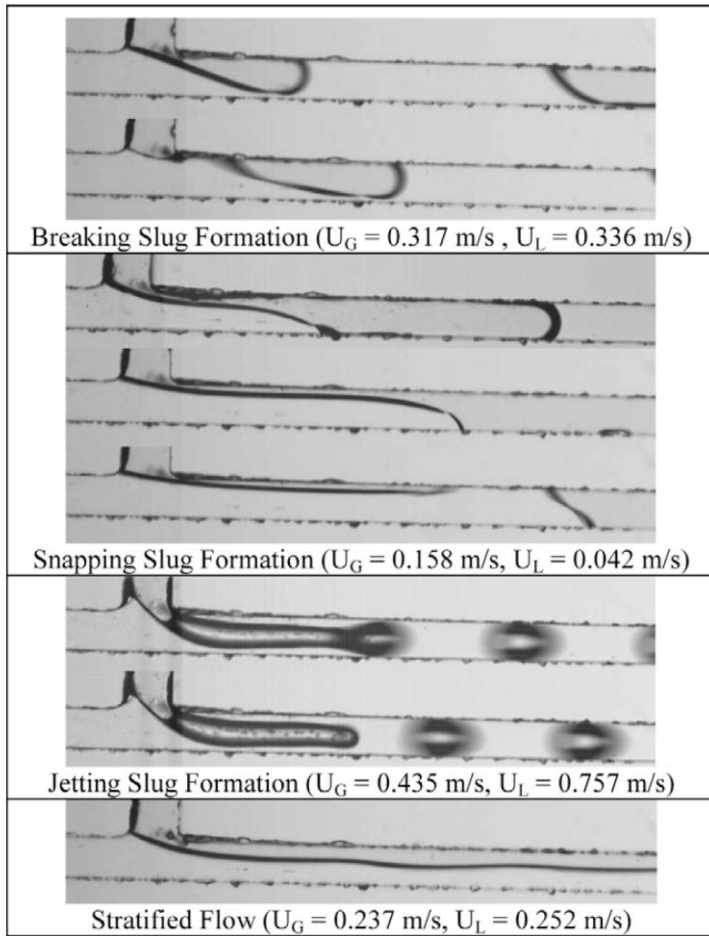Figure 4: Calculated inlet gas pressure as a function of superficial velocities

Breaking Slug Formation (U_G = 0.317 m/s , U_L = 0.336 m/s)
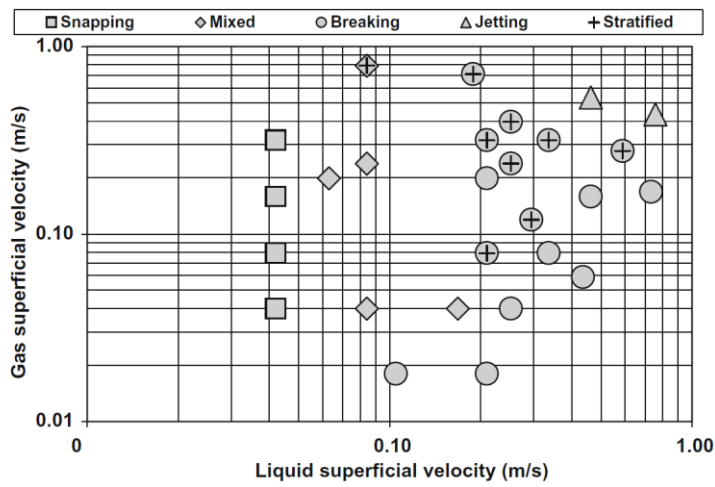
Snapping Slug Formation (U_G = 0.158 m/s, U_L = 0.042 m/s)

Jetting Slug Formation (U_G = 0.435 m/s, U_L = 0.757 m/s)

Stratified Flow (U_G = 0.237 m/s, U_L = 0.252 m/s)

Figure 5: Experimental Flow Patterns

Figure 6: T-junction flow pattern map

Maximum void fraction ($U_G = 0.712$ m/s, $U_L = 0.189$ m/s, $\varepsilon = 0.735$)

Minimum void fraction ($U_G = 0.059$ m/s, $U_L = 0.463$ m/s, $\varepsilon = 0.127$)
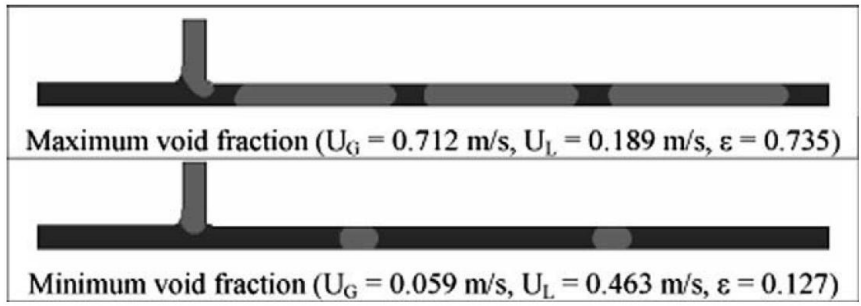
Figure 7: Numerical void fraction comparison
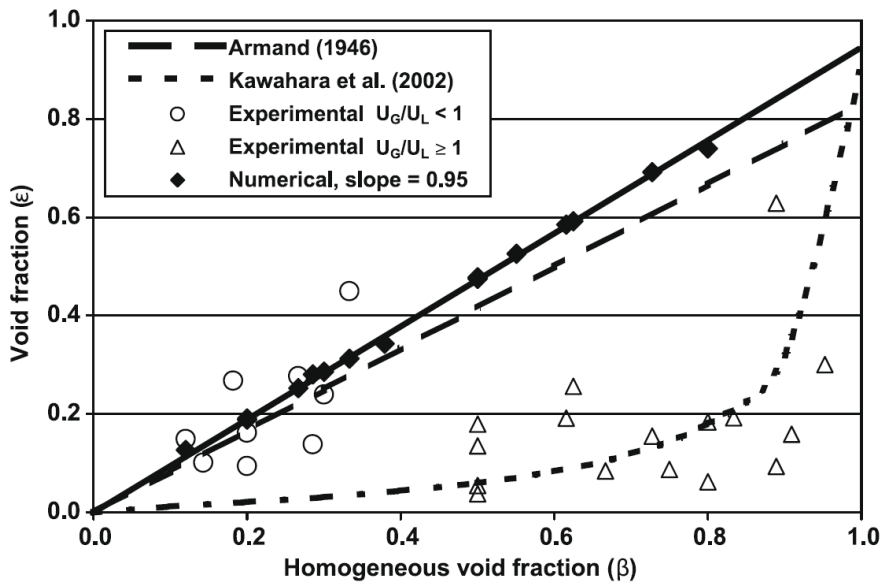
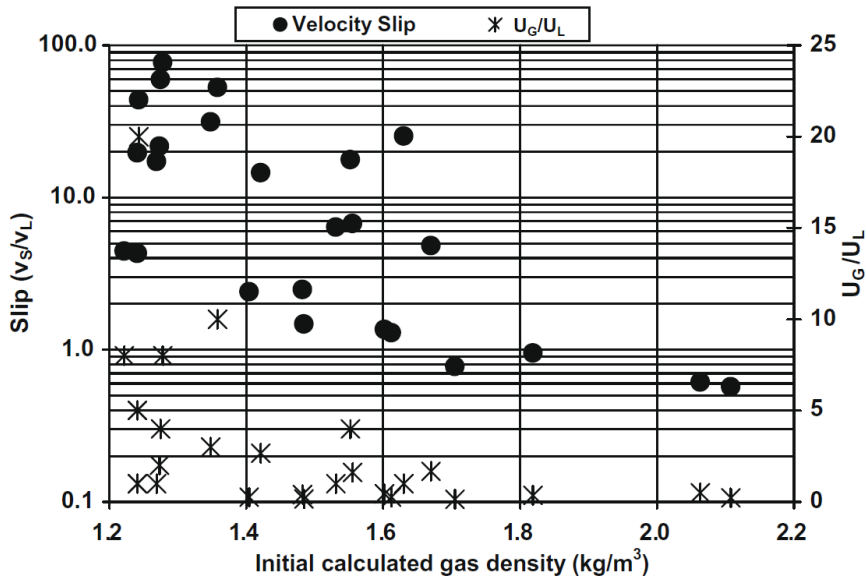Figure 8: Void fraction comparison

24
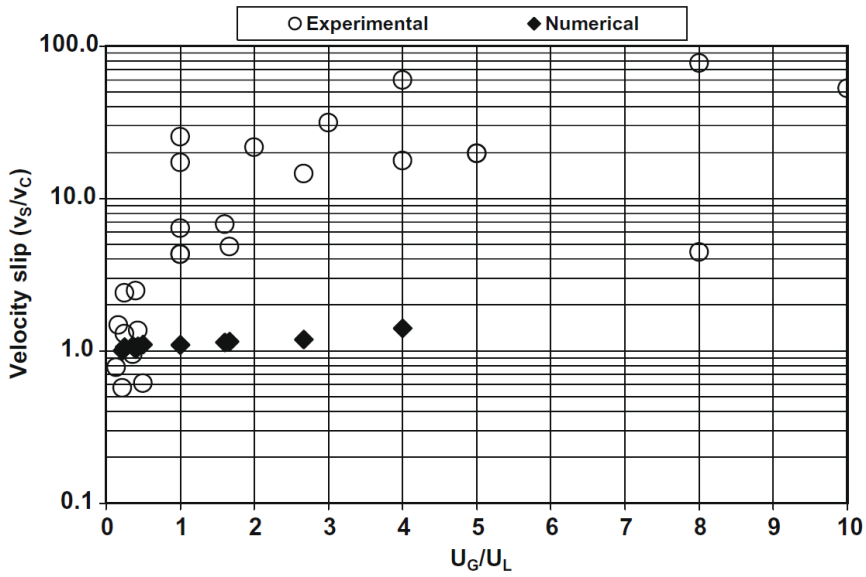
Figure 9: Velocity slip comparison

Figure 10: Effect of gas pressure build-up on velocity slip and relation to flow rate ratio
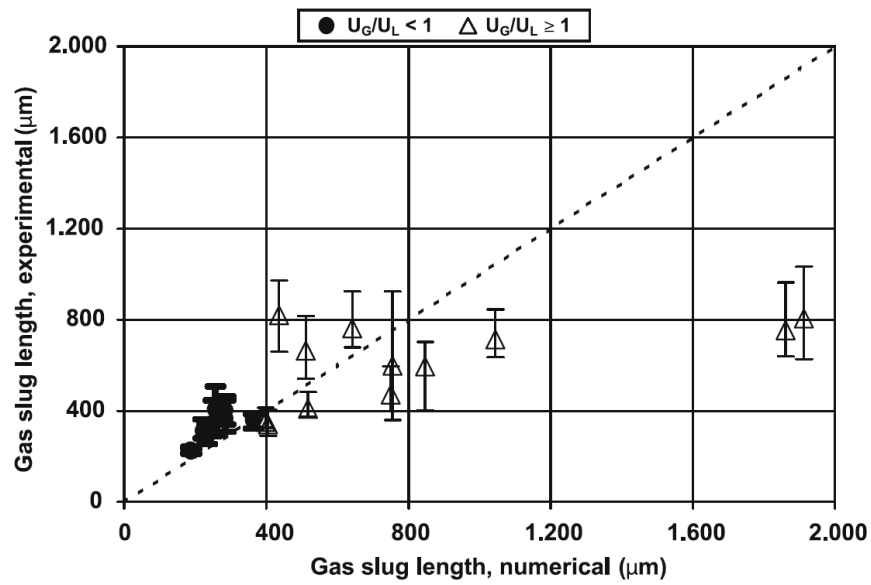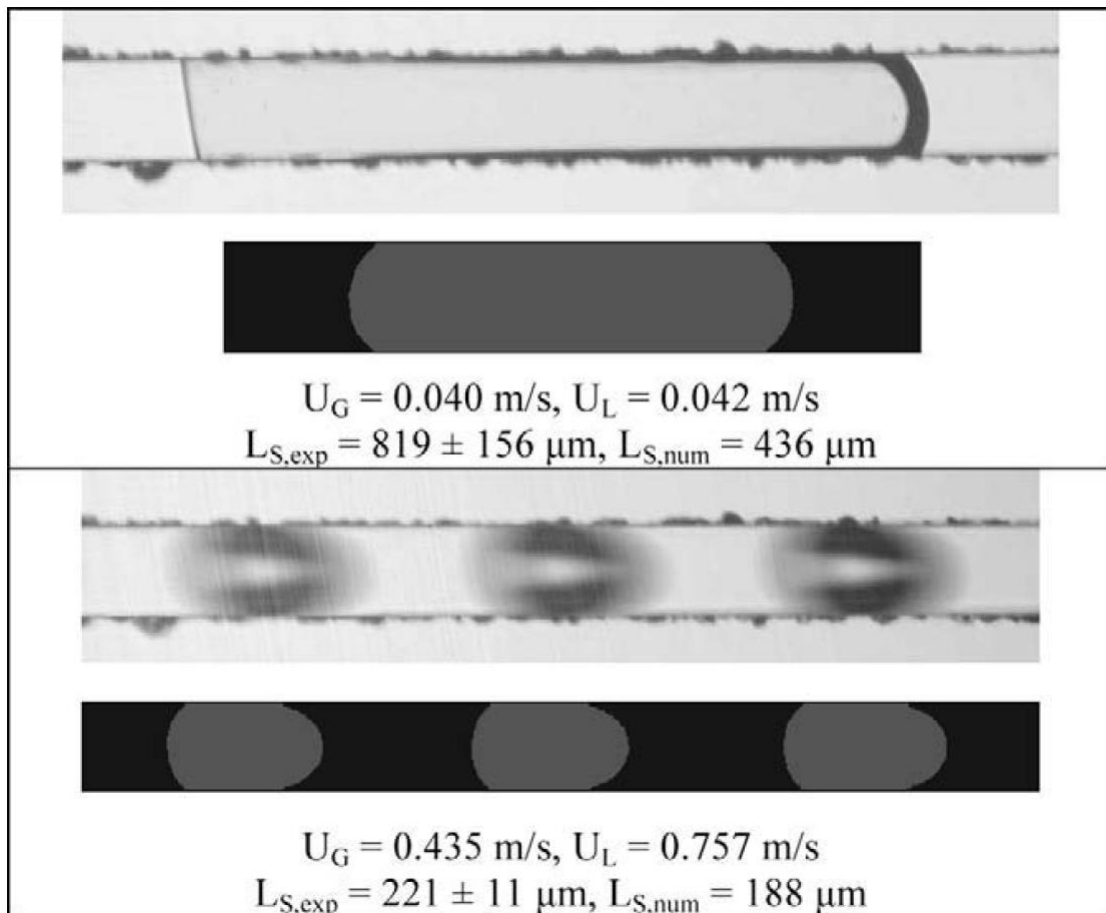
Figure 11: Gas slug length comparison

$U_G = 0.040$ m/s, $U_L = 0.042$ m/s
$L_{S,exp} = 819 \pm 156$ μm, $L_{S,num} = 436$ μm

$U_G = 0.435$ m/s, $U_L = 0.757$ m/s
$L_{S,exp} = 221 \pm 11$ μm, $L_{S,num} = 188$ μm

Figure 12: Comparison of experimental and numerical gas slug lengths
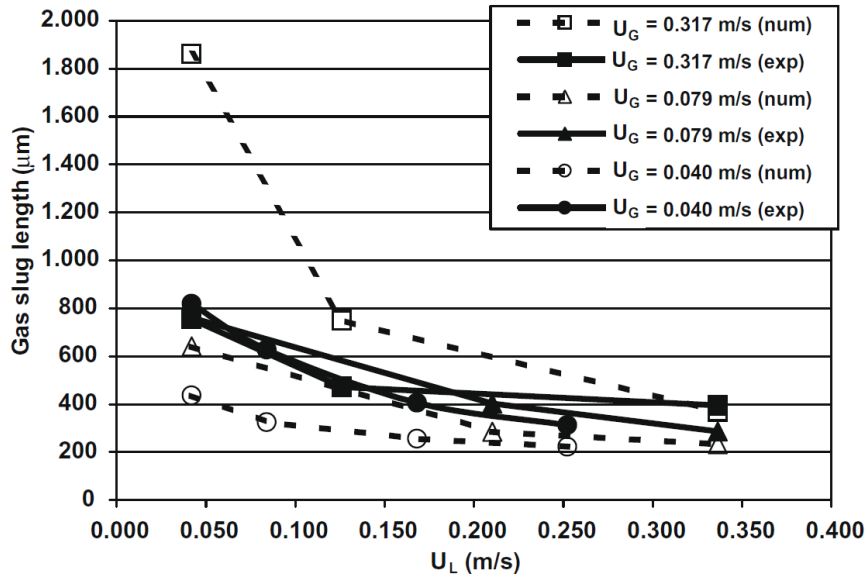
Figure 13: Comparison of experimental and numerical gas slug lengths as a function of flow rates

$U_G = 0.059$ m/s, $U_L = 0.463$ m/s
$A_S = 96\%$

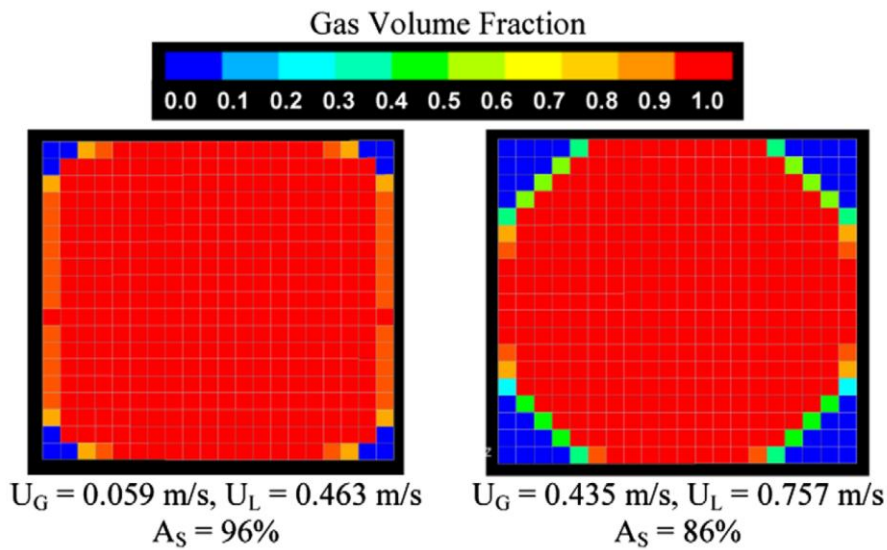$U_G = 0.435$ m/s, $U_L = 0.757$ m/s
$A_S = 86\%$

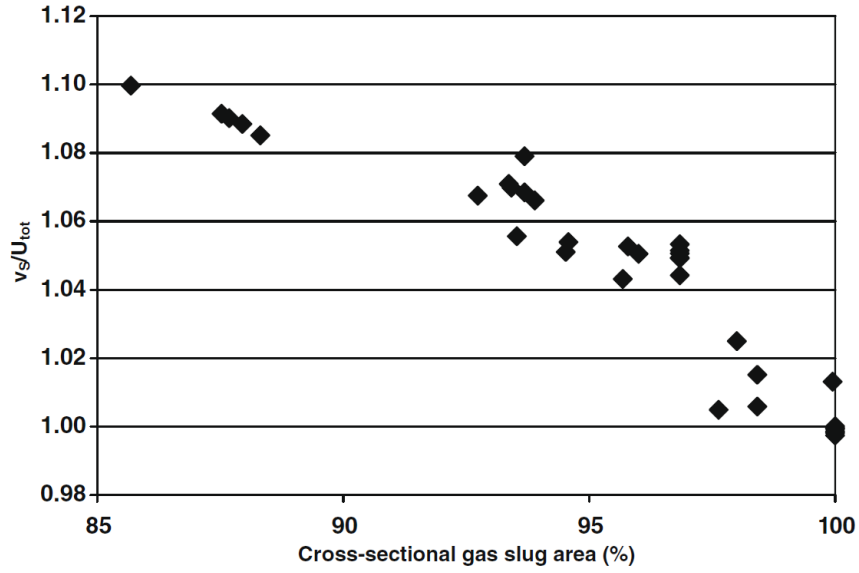Figure 14: Cross-sectional gas slug area comparison from numerical results

Figure 15: Gas slug velocity ratio versus cross-sectional gas slug area from numerical results

LIST OF TABLES

Table 1: Ranges of non-dimensional flow parameters

	Minimum	Maximum		Minimum	Maximum
$Bo = \dfrac{g(\rho_L - \rho_G)D_h^2}{\sigma}$	0.001704	0.001706	$Ca = \dfrac{\mu U_{tot}}{\sigma}$	0.0012	0.0171
$We_G = \dfrac{\rho U_G^2 D_h}{\sigma}$	6.5×10^{-7}	1.3×10^{-3}	$We_L = \dfrac{\rho U_L^2 D_h}{\sigma}$	2.7×10^{-3}	8.8×10^{-1}
$Re_G = \dfrac{\rho U_G D_h}{\mu}$	0.15	7.13	$Re_L = \dfrac{\rho U_L D_h}{\mu}$	4.7	85.4